IEEE Access
Multidisciplinary | Rapid Review | Open Access Journal

Received 11 April 2023, accepted 29 April 2023, date of publication 8 May 2023, date of current version 16 May 2023.

Digital Object Identifier 10.1109/ACCESS.2023.3273927

APPLIED RESEARCH

Electrical Model of a Membraneless Micro Redox Flow Battery–Fluid Dynamics Influence

ALBERTO BERNALDO DE QUIRÓS[1,2], ALBERTO E. QUINTERO[2,3], AIRÁN FRANCÉS[1], (Member, IEEE), ANGE A. MAURICE[3], AND JAVIER UCEDA[1], (Life Fellow, IEEE)

[1]Centro de Electrónica Industrial, Universidad Politécnica de Madrid, 28040 Madrid, Spain
[2]Research and Development Department, Micro Electrochemical Technologies S.L., 28919 Leganés, Spain
[3]Departamento de Ingeniería Térmica y de Fluidos, Universidad Carlos III de Madrid, 28911 Leganés, Spain

Corresponding author: Alberto Bernaldo de Quirós (a.bernaldodequiros@alumnos.upm.es)

This work was supported in part by the Industrial Doctorate Program of the Comunidad de Madrid under Grant IND2018/AMB-9616.

ABSTRACT Membraneless micro redox flow batteries are an incipient technology that has been shown to extend some properties of traditional redox flow batteries. Due to their microfluidic scale and the absence of membrane, the fluid dynamics operation is critical in the electrical response. In this work, an electrical model is established to evaluate the influence on three battery performance metrics: steady-state power, power transient dynamics, and mixing and self-discharge losses. First, an equivalent electrical circuit, derived from a state-of-the-art regular battery equivalent circuit, is defined by studying the influence of flow changes on its impedances and source, aggregating it as a variable. Then, empirical data are used to demonstrate the proposed equations defining the variation of the electrical response relative to fluid dynamics, and their parameters are identified with grey box methods. The steady-state power model incorporates the interphase position, extending conventionally used redox flow batteries expressions, such as Faraday´s Law and Nersnt´s equation, for the membraneless analysis. A transient response model is built, which becomes effectively relevant in intermittent power applications (such as many renewable energy storage ones). Finally, mixing and self-discharge losses are evaluated with the variation state of charge at the outputs of the cell, using spectrophotometry measurements, and compared with flowmeter mixing values. This demonstrates that flow-rate values can provide a precise quantification of these losses. The electrical model with dependent parameters from the three fluid dynamics analyses can be used to evaluate the performance of micro membraneless redox flow batteries and their response to fluidic operation.

INDEX TERMS Battery efficiency, electric equivalent model, grey box identification, microfluidics, redox flow battery.

I. INTRODUCTION

Redox Flow Battery (RFB) is an energy storage technology with properties such as long life cycle, low degradation, excellent scalability, cost-effectiveness, high depth of discharge, and an architecture with power decoupled from energy [1], [2]. This characteristic has been exploited since their early developments in the previous decades [3], [4], and especially in the current global energy transition scenario, where they are one of the preferred solutions for grid integration with intermittent energy sources, such as wind and solar photovoltaic renewable sources [5], [6]. Several different chemistries exist for RFB electrolytes, but Vanadium Redox Flow Batteries (VRFB) have proven to be the most mature technology in terms of industrialization and commercial applications [7].

Advances in microfabrication, together with the growing interest in microfluidics, have enabled the design of micro-scale redox flow reactors [1], [8]. The most defining feature of these solutions is the absence of a membrane, made possible by passing the electrolytes through the reactors in a laminar regime [9], [10], which prevents the flows from

The associate editor coordinating the review of this manuscript and approving it for publication was Zhe Zhang.

mixing and creates an interphase between the two species that minimizes the advective mixing. Some of these remarkable works are described in [11], [12], [13], [14], and [15]. These membraneless reactors can improve some of the characteristics of conventional RFB by operating with lower internal ohmic resistance and using a cheaper and simpler manufacturing method [16].

Several works have addressed the electric characterization of conventional redox flow batteries by proposing different equivalent electrical circuits that match the RFB responses to electrochemical impedance spectrometry [17], [18], [19], [20], [21]. These equivalent circuits consist of a source and a combination of impedances of different types and in different configurations. The values of the circuit elements depend on fixed structural parameters (electrode capacity and resistance, internal resistance, etc.), and others may also vary with operational variables such as state of charge (SOC) [19], pumping power, or flowrate [18]. Some works on equivalent electric circuits have used fractional order models for other types of batteries and supercapacitors [22], [23], which allow a more versatile structure to better reproduce the real behaviour of physical systems, using non-integer order derivatives together with traditional resistors, capacitors, and inductors. This methodology has not been applied to the equivalent circuits of redox flow batteries. Specific equivalent circuits for microfluidic membraneless RFB cannot be found in the literature, as their electrical dynamic response has not yet been studied in depth for grid integration.

Analysis, simulation, and mathematical modelling have been an important field of research for conventional RFB. Multi-physics and multiscale models cover areas such as electrochemical reactions [24], flow rate optimization [25], [26], state of charge [27], [28], open circuit voltage [29], as well as thermal effects [19]. These models range from pure analytical approaches such as [24], to parameters estimation with techniques such as extended Kalman filter [30], or more recently to the use of machine learning structures such as deep neuronal networks [31]. Likewise, for membraneless microfluidic reactor designs there has been an important effort to model their behaviour, not only with the aim of using them in these micro reactors, but also to extrapolate the knowledge from a more controlled and reduced experimental framework to the conventional batteries. This is especially notable in the study of mass transfer [32], [33] and diffusive mixing and self-discharge reactions [34]. The effects of channel and the electrode geometrical configurations have also been analysed [35].

In this work, the influence of the fluid dynamics of a membraneless microfluidic redox flow battery on its electrical response is studied. It is intended to demonstrate the critical need for optimal fluid operation and characterize the electrical performance by modelling the steady-state power value, the dynamics for transient power response, and quantifying the mixing and self-discharge losses. This can be used to obtain battery efficiency metrics with parameters that are not linked to the fluid dynamics in previous state-of-the-art models.

Furthermore, it is noted that previous designs [11], [12], [13], [14], [15] show the need of a deeper analysis of the influence of flow control due to their known suboptimal operating conditions: use of syringe pumps that may introduce pulsations, not considering possible manufacturing disturbances or any change in fluid properties. Different designs have been compared [36], but how operating conditions of the same design influence the electrical response has not been modelled.

As for the steady-state power, the conventional analysis consisted of using Faraday's law as the expression defining the electrical power associated with certain reactor electrolyte flows [37]. However, in this work, it is proven that the relationship of steady-state power to the net renovation flow in the reactor is incomplete for the membraneless case. Experimental data are used to compare the two proposed models, one that only depends on the net renovation of the species in the reactor (as indicated by the flow term in Faraday's law), and another that adds the interphase position correction. Both models are identified with grey box modelling techniques [38]. A model for the transient dynamic power response is proposed using a similar methodology, with its parameters identified and validated using experimental data.

Mixing and self-discharge losses are critical for reactors in which there is no separating membrane to prevent them. Therefore, they have been carefully studied in works considering mass transfer and diffusive mixing [32], [34]. In this work, the objective is limited to obtaining a model that correlates flow measurements with the change in electrolyte species concentration (state of charge), using spectrophotometry techniques as in other works [39], [40]. This correlation then can be incorporated into the fluid dynamics analysis of battery electric performance.

Hence, the contribution of this work to membraneless redox flow batteries is to present for the first time an equivalent electric circuit model for this type of batteries by adapting models of regular ones. The other main contribution is to study empirically the influence of fluid dynamics on this circuit. Electrochemical impedance spectrometry is used to identify which elements of the novel equivalent circuit vary with fluid dynamics. Empirical power experiments show the influence of the position of the liquid interphase on the available power beyond the conventional Faraday's law analysis for steady state response. Dynamic response is also modelled from experimental data. Spectrophotometry measurements correlate state-of-charge changes due to mixing and self-discharge with the working flows. It is demonstrated how critical fluid operation is and how this model can be used in optimizing battery performance.

This paper is organized as follows. Section II details membraneless micro redox flow batteries, the cell and complete system used in this work, and the equivalent electrical

circuit employed. Section III describes the models for the influence of fluid dynamics on the electrical power, both steady-state value and transient response dynamics, and the methodology for identifying the parameters of the proposed grey box model equations. Section IV explains how mixing and self-discharge losses are modelled from experimental data, correlating flowmeter and spectrophotometry data. The results of the identification of the proposed models, validation with real data, and comparison among different hypothetical operating conditions are discussed in Section V. Finally, conclusions are detailed in Section VI.

II. MICRO REDOX FLOW BATTERY

Membraneless microfluidic redox flow batteries share the same basic structure as conventional ones. They consist of two liquid electrolytes flowing from two separate tanks through a reactor where electrochemical charge or discharge reactions take place, and back to their respective tank. In these tanks, electrochemical energy is stored as a difference in the redox potential of the species present in each of the electrolytes. Therefore, battery capacity is proportional to the volume of electrolytes in these tanks, while battery power depends on reactor design (internal single cell design, electrode active area, number of cells, etc.) and the number of these reactors (more than one may be used for a battery system) [1]. Their architecture scheme is shown in Fig. 1.

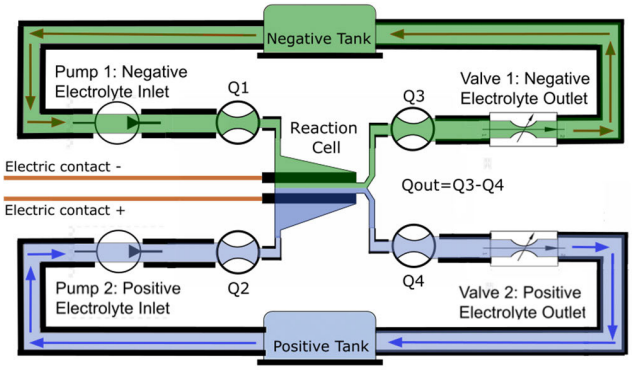

FIGURE 1. System scheme, with reaction cell, tanks, pumps connected to the inlets of the cell, valves at the outlets, and flowmeters and arrows signalling negative and positive electrolyte flows (Q1 to Q4).

The differences between conventional and micro concepts become more significant in the fluid system that pumps and controls the electrolytes and in the reactor design. For the fluid system, the micro membraneless designs use microfluidic technology and instrumentation, which means that pumps, valves, and all the possible actuators required, as well as sensors, tubing, and piping are built to operate in the microliters per minute range or less, with a Reynolds number below 1000 that can guarantee laminar flow regime.

The reactor design consists of two symmetrical halves in which each electrolyte flows in contact with an electrode that drives the reaction energy to the external electric circuit during discharge operation, or vice versa when charging. Conventional batteries use a selective ion-exchange membrane that keeps the two electrolytes physically separated, but ionically connected, so that protons can be exchanged across them. The absence of this element in micro designs determines the entire reactor design, since the flows through the reactor need to be in contact at a controlled interphase that keeps electrolytes separated. The internal ohmic resistance can be reduced with this configuration. In terms of cost, it also benefits from savings in membrane costs, both in terms of material and replacement of this element [41]. This, coupled with rapid fabrication and on-chip integration capability, can lead to a more cost-effective solution [12]. However, these designs have presented drawbacks for their industrialization, as it becomes challenging to ensure the correct distribution of reactants as the number of cells increases [8]. Applications that benefit from their higher surface to volume ratio in micro solutions, as well as the general characteristics of conventional RFB, need to scale up several cells in a stack to achieve higher power configurations.

In this work, the reactor design is a Y-junction cell based on the one presented in [42], which is a continuation of the work done in [14] and [15]. Further details on the fabrication of the device can be found in this literature, although the main structure is presented below. The reactor consists of three parts: microfluidic channel structure, electrodes, and glass substrate. The microfluidic channels are made of polydimethylsiloxane (PDMS), which by soft lithography replicates the channels of a plastic template (fabricated with the Asiga Max UV photolithography 3D printer). This PDMS structure has four holes to place tubing for the two inlets and two outlets. It also has two channels to place electrodes, which are made of carbon paper (Toray TP-090-T5). The dimensions of the electrode are 10 mm long, 1 mm wide, and 0.28 mm thick. They are spaced 0.75 mm apart. Finally, the PDMS microchannels with the electrodes placed in their respective channels are bonded to the glass (regular microscope glass slide) by applying a vacuum plasma treatment (using Harrick Plasma cleaner PDC-32G-2) to both surfaces. This seals the microfluidic cell. A scheme of the cell and an actual image of the cell are shown in Fig. 2.

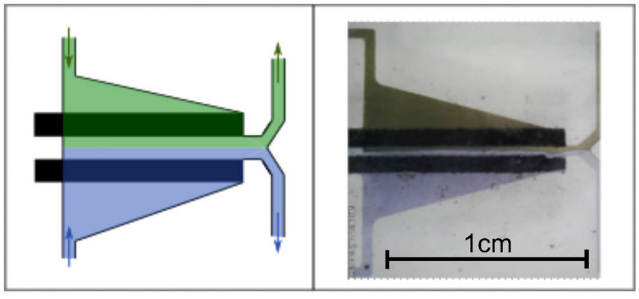

FIGURE 2. (Left) Schematic of the reaction cell with electrolytes interphase (diffusion is not depicted) (Right) Actual cell during operation.

The electrolytes are vanadium redox couples, commonly denominated as V(II)/V(III) and V(IV)/V(V). The anodic and

cathodic reactions for them, described in [43], are:

$$V^{3+} + e^- \leftrightarrow V^{2+} \quad E^0 = -0.496V \ vs \ SCE \tag{1}$$

$$VO_2{}^+ + 2H^+e^- \leftrightarrow VO^{2+} + H_2O \quad E^0 = -0.750V \ vs \ SCE \tag{2}$$

The system architecture also includes pumps at the inlets, propelling each electrolyte from its respective tank to the cell. These micropumps (Bartels-mikrotechnik Mp6-liq) operate on a peristaltic principle, with two chambers deflecting a membrane by the force of a piezoelectric. The high frequency pulses and small displacement of the piezoelectric generate a differential pressure that produces an effective flow. By modifying the frequency and voltage of the electrical wave applied to the piezoelectric, the flow rate can be regulated. These flow rates at the inlets, as well as that of the cell outlets, are measured with microfluidic flowmeters (Sensirion SLI-1000) to give feedback to the actuators and close the regulation loops. The electrolyte flow on the negative inlet side is denoted Q_1, the electrolyte flow on the positive inlet side is Q_2, and the difference between the flows on the negative (Q_3), and positive (Q_4) sides at the outlets is denominated Q_{out}. The outlet flows are regulated by pneumatic valves that narrow their internal channel proportionally to the air pressure applied to them. These valves are manufactured in an original design using 3D printing methods. The use of all the described instrumentation allows a continuous recirculation operation of the electrolytes. The actual system used is shown in Fig. 3.

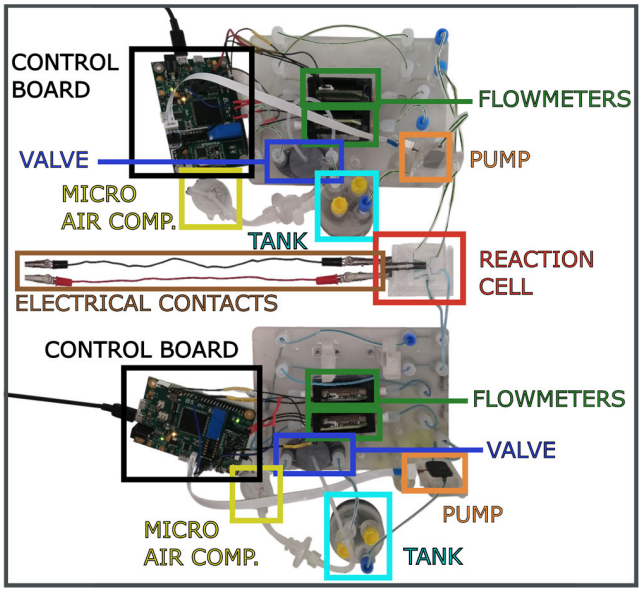

FIGURE 3. Actual photo of the system, with reaction cell and its electrical contacts; and the negative and positive parts, each with tank, pump, valve, flowmeters, micro air compressor, and control board.

A. ELECTRICAL EQUIVALENT CIRCUIT MODEL STRUCTURE

In this section, a proposed electrical equivalent circuit [20] of a conventional RFB is adapted and used as an approximation for the microfluidic membraneless case. This circuit consists of a structure that is repeated for each cell of a conventional battery stack, so only one of these structures is used as shown in Fig. 4. for the micro-cell.

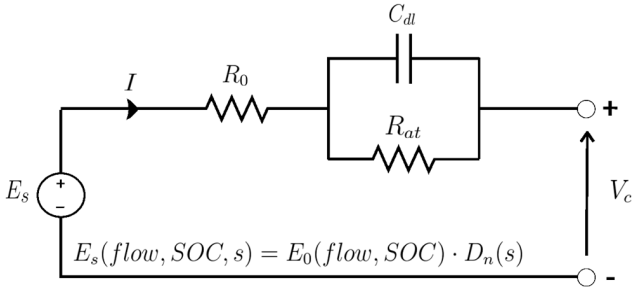

FIGURE 4. Equivalent electrical circuit of the membraneless micro redox flow battery based on the conventional model.

The circuit integrates a voltage source that models the ideal electromotive force of the battery, E_s, an ohmic resistance R_0 corresponding to the internal ohmic losses of the electrodes, electrolytes, and all electrical contacts (not the membrane in this case), and a parallel resistance-capacitance pair, in which the resistance R_{at} models the concentration and activation overpotentials, and the capacitance C_{dl} takes into account the electrical double layers at the contacts between the porous electrodes and the liquid electrolytes. The voltage at V_c corresponds to the accessible output of the cell. This is a simple model which, like other works in the literature [20], does not reflect shunt currents and the output power is considered before auxiliary power consumption (pumping system). In addition, mass transfer diffusion is excluded, which is usually modelled with a Warburg impedance. Electromotive force E_s is separated in the steady-state value E_o, and the time-dependent dynamic transfer function D_n.

The operating conditions have an impact in the parameters of the circuit. Temperature affects the voltage source E_s. State of charge and concentration again influence the voltage source and the resistance R_{at} and capacitance C_{dl}. These variables modify the voltage source, which in open circuit is set by the Nernst´s equation (here in its simplified form [19]):

$$E_{OCV} = E^\theta + \frac{2RT}{F} ln\left(\frac{SOC}{1 - SOC}\right), \tag{3}$$

where E^θ is the standard reduction potential for the given electrode, R is the universal gas constant (8.314 $Jmol^{-1}K^{-1}$), T the temperature in Kelvin, F the Faraday constant ($96487 Cmol^{-1}$), and SOC the state of charge of the battery which varies from 0 to 1.

The state of charge of a battery is usually defined [44] as the stored capacity (Q_{stored}) over the total theoretical capacity (Q_{total}):

$$SOC = \frac{Q_{stored}}{Q_{total}}. \tag{4}$$

In practice, it can be calculated in the negative electrolyte (SOC_-) as the concentration of the most negative vanadium

oxidation state (C_{neg}) over the total concentration of all vanadium species ($C_{\text{tot}-}$) in this negative electrolyte; or equivalently in the positive tank (SOC_+) as the concentration of the most positive vanadium oxidation state (C_{pos}) over the concentration of all vanadium species ($C_{\text{tot}+}$) in the positive electrolyte:

$$SOC_- = \frac{C_{neg}}{C_{tot-}}, \tag{5}$$

$$SOC_+ = \frac{C_{pos}}{C_{tot+}}. \tag{6}$$

In an ideal device with membrane these two equations should express the same SOC: only protons are exchanged across the membrane, so that concentrations vary at the same rate for both electrolytes. However, in real operation there are imbalances that are more pronounced in the membraneless case. This imbalance makes it useful to consider both SOC calculations in order to use the more limiting one.

In the following section, the influence of fluid dynamics on the different circuit elements is studied in order to determine how best to incorporate these effects into the equivalent model structure.

B. FLUID DYNAMIC INFLUENCE ON ELECTRICAL EQUIVALENT CIRCUIT

In order to study the fluid dynamics isolated from other operating conditions, the temperature is considered constant, and all experiments are performed in a controlled room temperature of 25 °C. The state of charge is also considered constant, working at an open circuit voltage of 1.42 V in all experiments.

Electrochemical Impedance Spectroscopy (EIS) makes it possible to identify the values of electrical elements of an equivalent circuit model by measuring the electrical impedance response of a circuit for different excitation frequencies. The measurements are usually presented on a Nyquist plot showing the real and imaginary part, and then the parameters of the selected equivalent electrical circuit are identified to fit this curve.

In this section, this method is used to see the changes in the circuit elements that modulate the impedance response, i.e. R_0, R_{at}, and C_{dl}. The EIS experiment is repeated with several different flow configurations to compare their Nyquist responses in 15 excitation frequencies in the range of 20 kHz to 1 Hz. This minimum frequency is not set below because diffusion effects start to become relevant, and therefore EIS measurements are not reliable for a reactor with flow through it, as noise starts to be present in the measurement. The frequency dependence of EIS measurement accuracy has been reported in previous work [45]. Furthermore, other works with microfluidic redox reactors use similar frequency ranges [15]. The flow configurations and their EIS response are shown in Fig. 5, where it can be observed how for the lower frequencies (final values at the right of the graph) some noisy values are present even before going below 1 Hz. Note that changes in these equivalent electrical elements

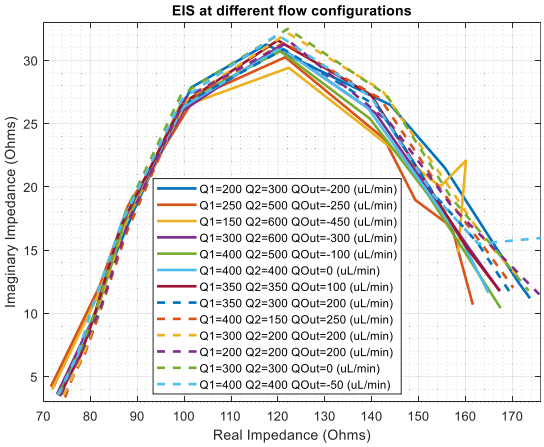

FIGURE 5. Nyquist plot of EIS experiments at different flow configurations.

due to flow configurations would be expected to modify the impedance response at different frequencies, and thus distort the entire EIS curve.

When comparing the data obtained at different flow configurations, it is observed that impedance response is very similar in all cases. This means that the fluid dynamics does not significantly affect the impedance parameters of the circuit.

However, in real operation, changes in the configuration of flow values and fluid dynamics are observed. This is shown in Fig. 6 where a constant voltage discharge is performed. In this experiment, all operation conditions are constant except the flow values. It is known that the state of charge of the electrolytes is the same for all the experiments as the electrolytes are not recirculated to the tanks at the cell outlets, so the volume in the tanks is not renewed.

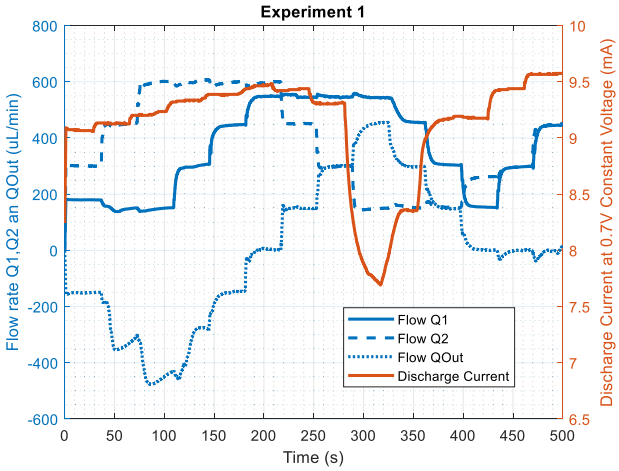

FIGURE 6. Constant voltage discharge experiment, with different flow configurations represented on the left axis by the three flows, and the maximum electric current on the right axis.

In this experiment, it becomes evident that the flow changes influence the electrical response of the cell. The dynamics of this experiment is driven by the whole equivalent

circuit response and the time scale of the flow steps. Since EIS measurements do not show significant changes in impedance value with varying flow configurations, it is decided to model this influence on the equivalent circuit as a variable for the voltage source function. Accordingly, the current variations measured at the cell output terminals are explained by this net power variation.

III. ELECTRIC SOURCE POWER VS FLUID DYNAMICS

In this section, the variation of the electrical source power with changes in fluid dynamics is studied. As can be deduced from the previous section, fluid dynamics is introduced as a variable in the equivalent circuit that modifies the voltage source.

This voltage source is also influenced by the state of charge of the electrolytes and the cell design. In order to isolate these other variables from the measurement, in each experiment the variables are converted to a relative measure from 0 to 1. This is done by dividing each value by the maximum for that particular SOC and cell design. The maximum power values are defined as those obtained above the maximum necessary electrolyte renovation in the reactor: for this cell design this value is effectively $800\mu L/min$. This allows to have a model of the influence of fluid dynamics and how flow operation affects battery performance, rather than modelling absolute power, which is out of the scope of this work.

A. STEADY-STATE

Steady-state power measurements are made at the battery output terminals. This power is different from the equivalent power at the voltage source of the circuit. Experiments are performed by measuring the current at constant voltage at the output terminals, and the equivalent steady-state source voltage is calculated using:

$$E_0 = V_c + I.Z_{circuit} = V_c + I.(R_0 + R_{at}). \tag{7}$$

This means that both the influence of the fluid on the steady-state source voltage and the battery power can be described from the response of the electric current to the fluid operation in constant voltage experiments.

Nernst´s equation describes the open-circuit source voltage of the equivalent circuit as introduced, and Faraday´s law relates the amount of chemical reaction of the active species (i.e., the volume of electrolytes) to the magnitude of the electrical charge passing through the electrodes. Applying Faraday´s expression to a time differential yields an equation that defines the minimum electrolyte flow for a given electric current [36]:

$$Q = \frac{2bN_{cell}.\mathrm{I}}{zFc_{vanadium}.SOC_{min}}, \tag{8}$$

where Q is the electrolyte flow rate that guarantees the minimum species renovation in the reactor, b is the sign factor that is 1 for charging and -1 for discharging, N_{cell} is the number of reactor cells, $i\,(t)$ is the net charge/discharge current, z is the number of electrons in the reaction (1 for the vanadium RFB), and SOC_{min} is the minimum state of charge of the electrolytes entering the reactor (in case they are different).

This can be rearranged to show that the maximum current is limited by the minimum inlet flow rate of the electrolytes:

$$I = Q_{min}\frac{zFc_{vandium}.SOC_{min}}{2bN_{cell}}. \tag{9}$$

This maximum current for (9) must match the value obtained from Nernst's equation (3) for the open circuit voltage, and the expression in (7) rearranged. Experimentally, it is measured using a high minimum inlet flow rate (above $800\mu L/min$) so that it does not limit the reaction.

$$I_{max} = \frac{E_{OCV} - V_C}{(R_0 + R_{at})}. \tag{10}$$

The expression in (9) indicates that, for a specific state of charge, at any instant, the value of the current depends on the minimum input flow for the renewal of the electrolyte's species multiplied by a constant factor. Considering constant temperature and state of charge, the relative current at an instant k is proportional to the minimum input flow by a factor K_F. The relative current I_r is defined divided by the maximum current for the working SOC.

$$I_r\,(k) = \frac{I}{I_{max}} = Q_{min}\,(k)\,.K_F\,. \tag{11}$$

This is true if only expressions for conventional batteries are used. Nevertheless, it can be proven that this is incomplete for microfluidic membraneless designs. In a constant voltage discharge experiment, without recirculation so that the state of charge of the electrolytes entering the reactor remains constant, the minimum inlet flow rate is kept at a fixed value while the ratio of the inlets is changed. In this scenario, the current is measured, and the results are shown in Fig. 7.

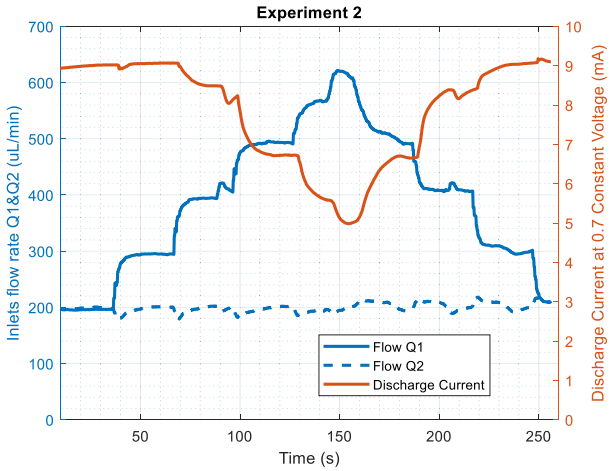

FIGURE 7. Constant voltage discharge experiment, with one of minimum inlet flow rates constant and modifying the fluidic interphase by changing the other inlet flow (left axis), and relative current output (right scale).

It is deduced that minimum input flow is not the only variable that defines the current. In membraneless cell designs, operating the flow at a correct ratio is critical to guarantee

laminar flows that form a centered interphase that avoids electrolyte mixing and minimizes advective mixing. Moreover, this experiment shows that interphase deviation due to changes in the ratio between the inlet flows influences the output current and, consequently, the available cell power.

To account for this effect, an equation is proposed including interphase effects for an instant k relative to the maximum current:

$$I_r(k) = Q_{min}(k).K_F - ratio_{In}(k) * K_{ratioIn} - ratio_{Out}(k) * K_{ratioOut}, \quad (12)$$

where $K_{ratioIn}$ and $K_{ratioOut}$ are constants to empirically quantify the power losses caused by interphase deviation. This interphase drift is calculated with an input and an output ratio, which are defined as:

$$\begin{aligned} if \left| \frac{Q_1(k) - Q_2(k)}{(Q_1(k) + Q_2(k))/2} \right| &> Threshold1: \\ ratio_{In}(k) &= \left| \frac{Q_1(k) - Q_2(k)}{(Q_1(k) + Q_2(k))/2} \right|^{exp} \\ else: ratio_{In}(k) &= 0, \end{aligned} \quad (13)$$

$$\begin{aligned} if \left| \frac{Q_{Out}(k)}{(Q_1(k) + Q_2(k))/2} \right| &> Threshold2 \\ ratio_{Out}(k) &= \left| \frac{Q_{Out}(k)}{(Q_1(k) + Q_2(k))/2} \right|^{exp} \\ else: ratio_{Out}(k) &= 0. \end{aligned} \quad (14)$$

This definition is based on the experimental behaviour observed in Fig. 7, where it is observed that the interphase deflection does not affect the output current until a threshold is reached, at which point an exponential loss occurs. The threshold, the exponential behaviour, and the rest of the parameters of this equation are identified from empirical experiments, using grey-box identification methods [38], and the results are discussed in Section V.

B. TRANSIENT DYNAMICS

The impedances of the equivalent electric circuit introduce a dynamic response to the electrical output. In the proposed circuit, where the voltage source varies with the flow, it also introduces a dynamic behaviour that needs to be modelled. Consequently, the steady-state power values for flow configurations discussed above do not change instantaneously but have a dynamic response.

The transient dynamics determines how the fluid dynamics must operate for any desired power transient response. This is how fast and stably power is available in the battery, supplying it in discharge mode and making it possible to convert it to energy storage when charging. This becomes important in applications that require frequent changes in power demand, typically intermittent energy sources such as wind and solar photovoltaic (very common applications for RFB). In this scenario, the power electronics must be designed by modelling the dynamic response of the battery to integrate it into the particular application.

Regarding the dynamic response of the impedances, it is modelled by curve fitting the EIS measurement that parametrizes the resistor and the capacitors of the circuit. This impedance transfer function, derived from the circuit in Fig. 3, is:

$$\frac{E_0(s)}{I(s)} = \frac{\frac{R_0+R_{at}}{R_{at}C_{dl}} + R_0 s}{\frac{1}{R_{at}C_{dl}} + s} \quad (15)$$

The transfer function of the impedance is used to transform the measured output current function into a curve at the voltage source. These transformed data are then used for the modelling of the electrical dynamics in relation with the fluid dynamics. The transfer function proposed to model these dynamics is:

$$D_n(s) = \frac{E_s(s)}{E_0(s)} = \frac{1}{1 + \tau.s} \quad (16)$$

where E_s is the instantaneous value of the voltage source, E_0 is the steady-state value corresponding to the power as modelled previously in the steady-state part, and τ is the time constant. It has been empirically verified that the parameter τ is different for increasing and decreasing flow rate changes. This equation is based on a low-pass filter with a response similar to that observed in the experimental data, as discussed in Section V. There, the value of the time constant (τ) is also obtained using grey-box identification for (16), and the fit to different experimental curves is calculated.

IV. SELF DISCHARGE AND MIXING LOSSES

The efficiency of membraneless RFB operation is severely limited by mixing and self-discharge losses. These losses have been studied and bounded, providing analytical expressions that can help in reactor design and to quantify capacity losses. However, these works such as [34] consider the optimal interphase positioning and do not evaluate how different flow configuration and fluid dynamics modify this capacity loss.

In this work, a first approach is made to correlate fluidic operation and mixing and self-discharge. The simplest approach is to consider the volume crossover directly proportional to the change in species concentration in the electrolytes. Diffusion mixing, which occurs at the interphase of the two electrolytes due to the difference in species concentration, is also considered. This is easily identified when the volume crossover is zero. Therefore, the equation correlating the state-of-charge loss and volume mixing is determined as:

$$SOC_{loss} = Diff + \%V_{mix} * K_m, \quad (17)$$

where $Diff$ is the fixed self-discharge loss mainly due to diffusion, K_m is a linear factor representing the proportionality between the state-of-charge loss (SOC_{loss}) and the percentage

of mixed liquid volume ($\%V_{mix}$). This percentage is:

$$\begin{aligned} &if\ (V_{Out1} - V_{Out2}) > (V_{In1} - V_{In2}) \\ &\qquad \%V_{mix} = \frac{(V_{Out1} - V_{Out2}) - (V_{In1} - V_{In2})}{2 * V_{Out1}} * 100 \\ &else \\ &\qquad \%V_{mix} = \frac{(V_{Out1} - V_{Out2}) - (V_{In1} - V_{In2})}{2 * V_{Out2}} * 100 \end{aligned} \tag{18}$$

Here, V indicates the volumes of the system, and the subscripts indicate whether the volume is measured at the inlet or outlet, and the numbers whether they belong to the negative or positive side (1 and 2 respectively).

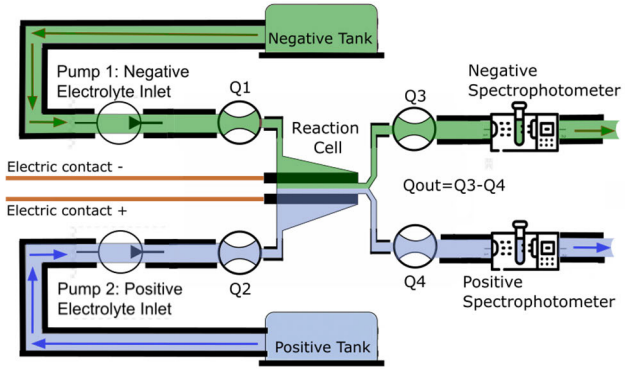

FIGURE 8. System configuration scheme for correlation between flow and mixing losses, with pumping system, reaction cell, flowmeters, and spectrophotometers. The cell outlets are not recirculated.

The scheme in Fig. 8 illustrates a configuration that allows empirical correlation between volumetric mixing flowmeter data and the change in state of charge provided by the spectrophotometers. These devices provide species concentration (state of charge) measurements using spectra calibration reference curves for each vanadium species. Since the electrolytes at the inlets are known to be at a certain state of charge, it is possible to calculate the change in species concentration. In the experiments, electrolytes at oxidation states V^{3+} and V^{4+} have been used for the negative and positive side, respectively, to simplify the spectrum analysis. Consequently, derived from equations (5) and (6), the state of charge for each electrolyte is calculated as the C_3 and C_4 concentrations of those two oxidation states:

$$SOC_{-} = \left(\frac{C_3}{C_3 + C_4}\right) \tag{19}$$

$$SOC_{+} = \left(\frac{C_4}{C_3 + C_4}\right) \tag{20}$$

The loss of state of charge is calculated as the initial state of charge (that is guaranteed to be equal in both electrolytes) minus the minimum of the SOC_{-} and SOC_{+} measured at the outputs.

The data is presented in the results section.

V. RESULTS AND DISCUSSION

A. ELECTRIC POWER VS FLUIDIC DYNAMICS: STEADY STATE

This section tests the models proposed in Section III.A. First, the parameters are identified using grey-box methods. Particularly, the regression has been implemented using the Gauss-Newton algorithm by means of Matlab.

This identification is performed for the parameters of equation (11), which correspond to the model obtained from the postulates of Faraday's law and Nernst's equation. As shown in Fig. 9, the best fit is not satisfactory, even when small corrections to the model (offset values) are introduced in an attempt to mitigate possible deviations due to noise in the data.

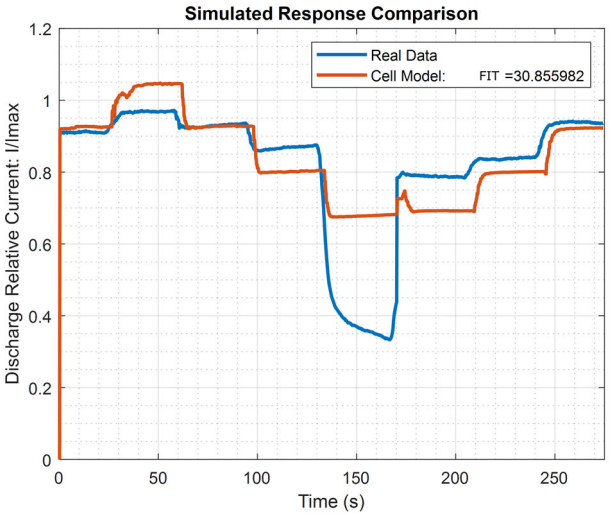

FIGURE 9. Simulated response for the model of equation (11) and real experimental data. The goodness of fit measurement is performed and indicated in the legend in percentage.

It is observed that the model only partially reproduces the general trend of the actual relative power. The fitness of the model is calculated using:

$$fit = 100\left(\frac{\|y - \hat{y}\|}{\|y - mean(y)\|}\right), \tag{21}$$

where y is the actual output data vector used as a reference, and $\hat{y}$ is the model output when excited with the actual input data. This measure indicates a low level of fitness for this model. This, together with the experiment reproduced in Fig. 7, makes clear the need for a more complex model, including quantification of the interphase goodness.

The model proposed in this work, detailed in expressions (12) to (14), includes the interphase influence as a correction. The parameters of its equations are again identified using Gauss-Newton regression algorithm. The best-found parameters are presented in Table 1, and the fit to the same real data used for their identification is shown in Fig. 10.

TABLE 1. Parameters values of the proposed equations (12)-(14).

Symbol	Quantity
K_F	$-5.5423\text{x}10^{-4}\ {}^{\mu L}/_{min}{}^{-1}$
$K_{ratioIn}$	0.0928
$K_{ratioOut}$	0.0781
$Threshold1$	0.5
$Threshold2$	0.5
exp	4

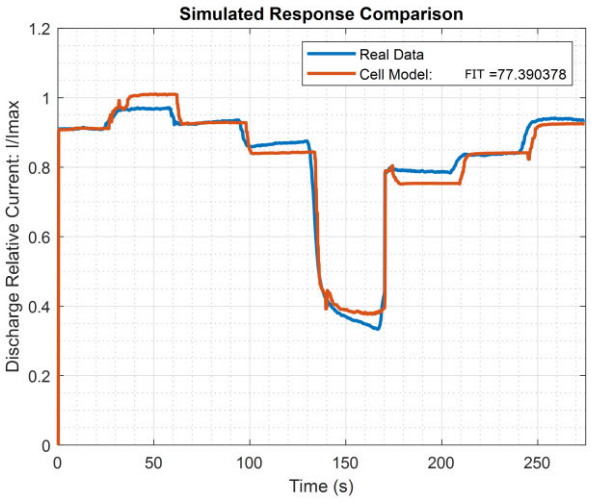

FIGURE 10. Simulated response for the proposed model from equations (12)-(14) with parameters from Table 1, and actual steady-state relative current experimental data. The fitness measure is indicated in the legend.

This model seems to be able to accurately represent the actual relative current performance of the battery, and is cross-validated with data from different experiments where flow operation is different. This is represented in Fig. 11.

The fitness of this experiment demonstrates that the identified model parameters are extendable for different conditions. The fitness measure is slightly lower than when using the same data for identification and validation, but it is still quite similar, and the model response is considered satisfactory. It should be noted that microfluidic devices, such as the reaction cell of this work, suffer from inconsistency due to multiple factors (temperature and pressure fluctuations, substrate deformation, etc.) [46], which reinforces the relevance of the obtained fitness measurements. It is shown that this model is valid for estimating relative electrical power from fluid dynamics operation data.

B. ELECTRIC POWER VS FLUIDIC DYNAMICS: TRANSIENT DYNAMICS

The proposed transient relative electric power dynamics is validated using experimental data in which periodic power steps are generated producing repetitive steps in the flow operating conditions. The flow steps are performed

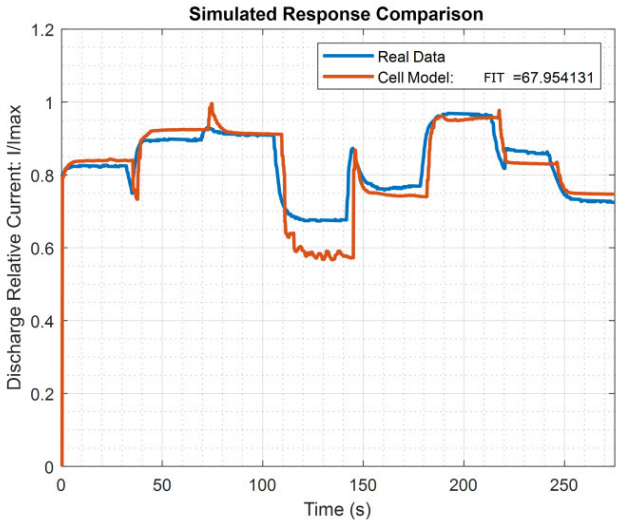

FIGURE 11. Simulated response for the model of equations (12)-(14) with the parameters of Table 1, and actual steady-state relative current experimental data. The fitness measure is indicated in the legend.

to produce different settling times and stability conditions. These different experimental conditions are used to find the optimal value of the time constant defined in (16), which, as explained, turns out to be different for increasing than for decreasing flow dynamics ($\tau = 1$ and $\tau = 1.333$ respectively). These experiments, in Fig. 12, are also used for model validation. Note that the minimum inlet flow rate is also plotted graphically for each experiment, so that different operating conditions and how their dynamics translate into the power output are better understood.

It is demonstrated that the proposed model with the identified values of the time constant reproduces the real dynamics, with settling and overshoot time close to the real ones, and NRMSE measurements indicating high fitness in all different conditions.

C. SELF DISCHARGE AND MIXING RESULTS

The proposed mixing experiment with the system configuration shown in Fig. 8 is performed with several different flow configurations to obtain different electrolyte mixtures. For each configuration, the mixing percentage by volume and state of charge are calculated.

Considering that the electrolytes at the inlets are at full state of charge, the state-of-charge losses are obtained by subtracting the limiting value of SOC value from the spectrophotometer at the outlets.

The results of the experiments are shown in Fig. 13, together with the plot of equation (17) with the parameters $Diff = 9.394$ and $K_m = 0.678$ adjusted to minimize root-mean-square error (RMSE).

It is demonstrated that the expression modelled in (17) reproduces the actual behaviour of the losses. The volume crossover together with the diffusion of active species can explain the main losses due to self-discharge. This constant

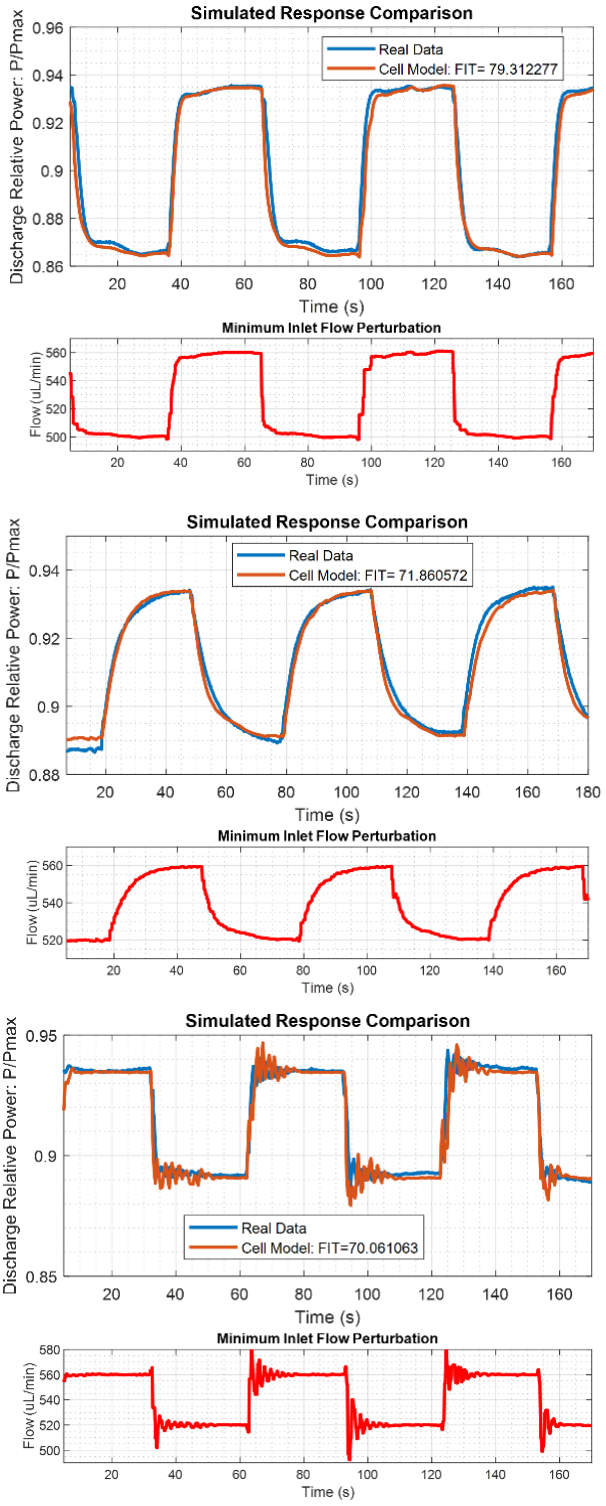

FIGURE 12. Simulated responses for the dynamic model and three real experimental transient power data. The fitness measure is indicated in each legend. The lower plot for each experiment shows the minimum inlet flow rate to better indicate the different experimental conditions for each dynamic response.

loss due to diffusion is one of the main drawbacks of membraneless operation, and it is concluded that it is necessary to improve the design used in [42]. Furthermore, it is

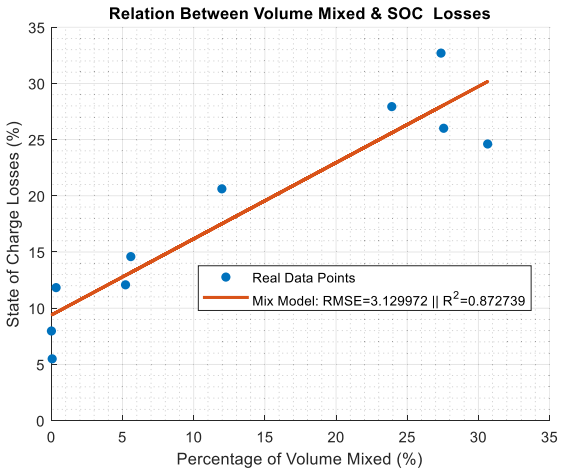

FIGURE 13. Relation between SOC losses and mixed volume, with experimental points and linear curve model fit indicated. Root-mean-square error and R^2 measurements are shown in the legend.

demonstrated that minimizing the volume error with proper flow control is critical for battery performance.

VI. CONCLUSION

In this work, models of the influence of microfluidic dynamics on the electrical response of a membraneless micro redox flow battery are presented. Three metrics are modelled: the influence of steady-state relative power, transient power dynamics, and mixing and self-discharge losses. First, an equivalent electrical model is proposed from existing conventional models. The fluidic influence on the equivalent impedances (without finding variations in this output impedance) and the open-circuit source are studied. Then, based on the results, the equivalent circuit is modified by adding fluid dynamics parameters as variables of the source.

The steady state of the relative power is studied empirically and it is demonstrated that modelling based on conventional analytical expressions is incomplete in describing the connection between fluidic operation and how power changes. Interphase depletion is included in the analysis with the proposed flow ratios. The transient dynamics are defined with transfer functions derived from the impedances of the equivalent electrical circuit, together with proposed dynamics for the influence on the power source of fluid dynamics. Finally, a model of mixing and self-discharge losses is designed by studying flowmeters and spectrophotometers measurements in a non-recirculating discharge experiment, in which the mixed volume and state-of-charge loss are correlated.

The parameters of the proposed equations are identified using grey-box regression methods. Experimental data are then used for validation, and the fitness measures indicate that the models for all three metrics are satisfactory. Therefore, they are valid for modelling the influence of fluid dynamics on the electrical response of the membraneless RFB. The proposed model can be a valuable tool to optimize the operation of membraneless micro redox flow batteries by taking into account the effect of fluid dynamics.

As future work, it is proposed to refine the flow ratios describing the interphase effect on steady-state power by modelling minor effects such as viscosity changes and small nonlinearities due to state-of-charge variations. It is also planned to study other equivalent circuit configurations, such as fractional order-based models. For mixing and self-discharge losses, further spectrophotometry experiments are planned to refine the diffusion effects in the model.

REFERENCES

[1] E. Sánchez-Díez, E. Ventosa, M. Guarnieri, A. Trovo, C. Flox, R. Marcilla, F. Soavi, P. Mazur, E. Aranzabe, and R. Ferret, "Redox flow batteries: Status and perspective towards sustainable stationary energy storage," *J. Power Sources*, vol. 481, Jan. 2021, Art. no. 228804.

[2] A. Aluko and A. Knight, "A review on vanadium redox flow battery storage systems for large-scale power systems application," *IEEE Access*, vol. 11, pp. 13773–13793, 2023, doi: 10.1109/ACCESS.2023.3243800.

[3] M. Skyllas-Kazacos, M. Rychcik, R. G. Robins, A. G. Fane, and M. A. Green, "New all-vanadium redox flow cell," *J. Electrochem. Soc.*, vol. 133, no. 5, p. 1057, May 1986.

[4] L. H. Thaller, "Electrically rechargeable redox flow cells," NASA, Washington, DC, USA, Tech. Rep., TM X-71540, 1974, pp. 1–5.

[5] C. Zhang, L. Zhang, Y. Ding, S. Peng, X. Guo, Y. Zhao, G. He, and G. Yu, "Progress and prospects of next-generation redox flow batteries," *Energy Storage Mater.*, vol. 15, pp. 324–350, Nov. 2018, doi: 10.1016/j.ensm.2018.06.008.

[6] P. Lu, P. Leung, H. Su, W. Yang, and Q. Xu, "Materials, performance, and system design for integrated solar flow batteries—A mini review," *Appl. Energy*, vol. 282, Jan. 2021, Art. no. 116210, doi: 10.1016/j.apenergy.2020.116210.

[7] Z. Huang and A. Mu, "Research and analysis of performance improvement of vanadium redox flow battery in microgrid: A technology review," *Int. J. Energy Res.*, vol. 45, no. 10, pp. 14170–14193, Aug. 2021, doi: 10.1002/er.6716.

[8] O. A. Ibrahim, M. Navarro-Segarra, P. Sadeghi, N. Sabaté, J. P. Esquivel, and E. Kjeang, "Microfluidics for electrochemical energy conversion," *Chem. Rev.*, vol. 122, no. 7, pp. 7236–7266, Apr. 2022, doi: 10.1021/acs.chemrev.1c00499.

[9] E. Choban, "Microfluidic fuel cell based on laminar flow," *J. Power Sources*, vol. 128, no. 1, pp. 54–60, Mar. 2004.

[10] K. Marma, J. Kolli, and K. T. Cho, "Membrane-less hydrogen iron redox flow battery," *J. Electrochem. Energy Convers. Storage*, vol. 16, no. 1, Feb. 2019, Art. no. 011005, doi: 10.1115/1.4040329.

[11] R. Ferrigno, A. D. Stroock, T. D. Clark, M. Mayer, and G. M. Whitesides, "Membraneless vanadium redox fuel cell using laminar flow," *J. Amer. Chem. Soc.*, vol. 124, no. 44, pp. 12930–12931, Nov. 2002.

[12] W. Lee, M. A. Goulet, and E. Kjeang, "Microfluidic redox battery," *Lab Chip*, vol. 13, pp. 2504–2507, Jan. 2013.

[13] J. P. Esquivel, P. Alday, O. A. Ibrahim, B. Fernández, E. Kjeang, and N. Sabaté, "A metal-free and biotically degradable battery for portable single-use applications," *Adv. Energy Mater.*, vol. 7, no. 18, Sep. 2017, Art. no. 1700275.

[14] E. Kjeang, J. McKechnie, D. Sinton, and N. Djilali, "Planar and three-dimensional microfluidic fuel cell architectures based on graphite rod electrodes," *J. Power Sources*, vol. 168, no. 2, pp. 379–390, Jun. 2007.

[15] E. Kjeang, R. Michel, D. A. Harrington, N. Djilali, and D. Sinton, "A microfluidic fuel cell with flow-through porous electrodes," *J. Amer. Chem. Soc.*, vol. 130, no. 12, pp. 4000–4006, Mar. 2008.

[16] K. M. Lisboa and R. M. Cotta, "On the mass transport in membraneless flow batteries with flow-by configuration," *Int. J. Heat Mass Transf.*, vol. 122, pp. 954–966, Jul. 2018, doi: 10.1016/j.ijheatmasstransfer.2018.02.002.

[17] Y. Zhang, J. Zhao, P. Wang, M. Skyllas-Kazacos, B. Xiong, and R. Badrinarayanan, "A comprehensive equivalent circuit model of all-vanadium redox flow battery for power system analysis," *J. Power Sources*, vol. 290, pp. 14–24, Sep. 2015, doi: 10.1016/j.jpowsour.2015.04.169.

[18] A. Bhattacharjee and H. Saha, "Design and experimental validation of a generalised electrical equivalent model of vanadium redox flow battery for interfacing with renewable energy sources," *J. Energy Storage*, vol. 13, pp. 220–232, Oct. 2017, doi: 10.1016/j.est.2017.07.016.

[19] B. Xiong, Y. Yang, J. Tang, Y. Li, Z. Wei, Y. Su, and Q. Zhang, "An enhanced equivalent circuit model of vanadium redox flow battery energy storage systems considering thermal effects," *IEEE Access*, vol. 7, pp. 162297–162308, 2019, doi: 10.1109/access.2019.2952212.

[20] A. Trovo, W. Zamboni, and M. Guarnieri, "Multichannel electrochemical impedance spectroscopy and equivalent circuit synthesis of a large-scale vanadium redox flow battery," *J. Power Sources*, vol. 493, May 2021, Art. no. 229703, doi: 10.1016/j.jpowsour.2021.229703.

[21] W. Guan and X. Huang, "A modular active balancing circuit for redox flow battery applied in energy storage system," *IEEE Access*, vol. 9, pp. 127548–127558, 2021, doi: 10.1109/ACCESS.2021.3112902.

[22] N. Chen, P. Zhang, J. Dai, and W. Gui, "Estimating the state-of-charge of lithium-ion battery using an H-infinity observer based on electrochemical impedance model," *IEEE Access*, vol. 8, pp. 26872–26884, 2020, doi: 10.1109/ACCESS.2020.2971002.

[23] J. Wang, L. Zhang, J. Mao, J. Zhou, and D. Xu, "Fractional order equivalent circuit model and SOC estimation of supercapacitors for use in Hess," *IEEE Access*, vol. 7, pp. 52565–52572, 2019, doi: 10.1109/ACCESS.2019.2912221.

[24] C. Blanc and A. Rufer, "Multiphysics and energetic modeling of a vanadium redox flow battery," in *Proc. IEEE Int. Conf. Sustain. Energy Technol.*, Nov. 2008, pp. 696–701, doi: 10.1109/ICSET.2008.4747096.

[25] S. König, M. R. Suriyah, and T. Leibfried, "Innovative model-based flow rate optimization for vanadium redox flow batteries," *J. Power Sources*, vol. 333, pp. 134–144, Nov. 2016, doi: 10.1016/j.jpowsour.2016.09.147.

[26] Z. Huang, A. Mu, L. Wu, and H. Wang, "Vanadium redox flow batteries: Flow field design and flow rate optimization," *J. Energy Storage*, vol. 45, Jan. 2022, Art. no. 103526, doi: 10.1016/j.est.2021.103526.

[27] B. Turker, S. A. Klein, E.-M. Hammer, B. Lenz, and L. Komsiyska, "Modeling a vanadium redox flow battery system for large scale applications," *Energy Convers. Manag.*, vol. 66, pp. 26–32, Feb. 2013, doi: 10.1016/j.enconman.2012.09.009.

[28] A. Clemente, M. Montiel, F. Barreras, A. Lozano, and R. Costa-Castello, "Vanadium redox flow battery state of charge estimation using a concentration model and a sliding mode observer," *IEEE Access*, vol. 9, pp. 72368–72376, 2021, doi: 10.1109/ACCESS.2021.3079382.

[29] K. W. Knehr and E. C. Kumbur, "Open circuit voltage of vanadium redox flow batteries: Discrepancy between models and experiments," *Electrochem. Commun.*, vol. 13, no. 4, pp. 342–345, Apr. 2011, doi: 10.1016/j.elecom.2011.01.020.

[30] M. R. Mohamed, H. Ahmad, M. N. A. Seman, S. Razali, and M. S. Najib, "Electrical circuit model of a vanadium redox flow battery using extended Kalman filter," *J. Power Sources*, vol. 239, pp. 284–293, Oct. 2013, doi: 10.1016/j.jpowsour.2013.03.127.

[31] J. Bao, V. Murugesan, C. J. Kamp, Y. Shao, L. Yan, and W. Wang, "Machine learning coupled multi-scale modeling for redox flow batteries," *Adv. Theory Simul.*, vol. 3, no. 2, 2019, Art. no. 1900167, doi: 10.1002/adts.201900167.

[32] M. N. Nasharudin, S. K. Kamarudin, U. A. Hasran, and M. S. Masdar, "Mass transfer and performance of membrane-less micro fuel cell: A review," *Int. J. Hydrogen Energy*, vol. 39, no. 2, pp. 1039–1055, Jan. 2014, doi: 10.1016/j.ijhydene.2013.09.135.

[33] J. Marschewski, P. Ruch, N. Ebejer, O. H. Kanan, G. Lhermitte, Q. Cabrol, B. Michel, and D. Poulikakos, "On the mass transfer performance enhancement of membraneless redox flow cells with mixing promoters," *Int. J. Heat Mass Transf.*, vol. 106, pp. 884–894, Mar. 2017.

[34] S. E. Ibáñez, A. E. Quintero, P. A. García-Salaberri, and M. Vera, "Effects of the diffusive mixing and self-discharge reactions in microfluidic membraneless vanadium redox flow batteries," *Int. J. Heat Mass Transf.*, vol. 170, May 2021, Art. no. 121022, doi: 10.1016/j.ijheatmasstransfer.2021.121022.

[35] M. Tanveer and K.-Y. Kim, "Effects of geometric configuration of the channel and electrodes on the performance of a membraneless micro-fuel cell," *Energy Convers. Manag.*, vol. 136, pp. 372–381, Mar. 2017, doi: 10.1016/j.enconman.2017.01.027.

[36] M. O. Bamgbopa, S. Almheiri, and H. Sun, "Prospects of recently developed membraneless cell designs for redox flow batteries," *Renew. Sustain. Energy Rev.*, vol. 70, pp. 506–518, Apr. 2017.

[37] G. Merei, S. Adler, D. Magnor, M. Leuthold, and D. U. Sauer, "Multiphysics model for a vanadium redox flow battery," *Energy Proc.*, vol. 46, pp. 194–203, Jan. 2014, doi: 10.1016/j.egypro.2014.01.173.

[38] T. Bohlin, *Practical Grey-Box Process Identification: Theory and Applications*. Berlin, Germany: Springer, 2006.

[39] M. E. Suss, K. Conforti, L. Gilson, C. R. Buie, and M. Z. Bazant, "Membraneless flow battery leveraging flow-through heterogeneous porous media for improved power density and reduced crossover," *RSC Adv.*, vol. 6, no. 102, pp. 100209–100213, 2016, doi: 10.1039/C6RA22608F.
[40] K.-H. Shin, C.-S. Jin, J.-Y. So, S.-K. Park, D.-H. Kim, and S.-H. Yeon, "Real-time monitoring of the state of charge (SOC) in vanadium redox-flow batteries using UV–Vis spectroscopy in operando mode," *J. Energy Storage*, vol. 27, Feb. 2020, Art. no. 101066, doi: 10.1016/j.est.2019.101066.
[41] G. Kear, A. A. Shah, and F. C. Walsh, "Development of the all-vanadium redox flow battery for energy storage: A review of technological, financial and policy aspects," *Int. J. Energy Res.*, vol. 36, no. 11, pp. 1105–1120, Sep. 2012, doi: 10.1002/er.1863.
[42] M.-A. Goulet and E. Kjeang, "Reactant recirculation in electrochemical co-laminar flow cells," *Electrochimica Acta*, vol. 140, pp. 217–224, Sep. 2014.
[43] D. R. Lide, *Handbook of Chemistry and Physics*, 90th ed. Boca Raton, FL, USA: CRC Press, 2010.
[44] Y. Yao, J. Lei, Y. Shi, F. Ai, and Y.-C. Lu, "Assessment methods and performance metrics for redox flow batteries," *Nature Energy*, vol. 6, no. 6, pp. 582–588, Feb. 2021, doi: 10.1038/s41560-020-00772-8.
[45] C. Iliescu, D. P. Poenar, and S. T. Selvan, "Frequency dependence on the accuracy of electrical impedance spectroscopy measurements in microfluidic devices," *J. Micromech. Microeng.*, vol. 20, no. 2, Feb. 2010, Art. no. 022001.
[46] O. J. Dressler, P. D. Howes, J. Choo, and A. J. deMello, "Reinforcement learning for dynamic microfluidic control," *ACS Omega*, vol. 3, no. 8, pp. 10084–10091, Aug. 2018.

ALBERTO BERNALDO DE QUIRÓS received the M.Sc. degree in automatic and robotics from Universidad Politécnica de Madrid (UPM), Spain, in 2016, where he is currently pursuing the Ph.D. degree in industrial mention in collaboration with the Company Micro Electrochemical Technologies S.L. His current research interests include the modeling and control of multivariable non-linear systems, focused on energy storage electronics and microfluidics applications.

ALBERTO E. QUINTERO received the M.Sc. degree in industrial mathematics and the Ph.D. degree in industrial organization and mechanical engineering from the Universidad Carlos III de Madrid (UC3M), Spain, in 2012 and 2016, respectively.

He is currently the Head of engineering with Micro Electrochemical Technologies S.L. He is also an Adjunct Professor of fluid mechanics with UC3M. His research interests include heat and mass transfer processes, nanotechnology, microtechnology, and microfluidics for energy storage systems in industrial applications.

AIRÁN FRANCÉS (Member, IEEE) received the M.Sc. and Ph.D. degrees in electrical engineering from Universidad Politécnica de Madrid (UPM), Spain, in 2012 and 2018, respectively.

He is currently an Assistant Professor with the Department of Electrical Engineering, UPM. He has participated in the European project XFEL, for two years, where he collaborated in the design and development of dc/dc power supplies for superconducting magnets. His current research interests include modeling, control and stability assessment of electronic power distribution systems, and smart grids.

ANGE A. MAURICE received the master's degree in material science and engineering from Institut National des Sciences appliquées de Lyon (INSA), France, and the Ph.D. degree in nanotechnology from Nanyang Technological University (NTU), Singapore.

He is currently a Postdoctoral Researcher with the Thermal and Fluid Mechanics Department, Universidad Carlos III de Madrid. His current research interests include microfluidics systems, spectroscopy methods, experimental calibration, and redox flow battery electrolytes for energy storage applications.

JAVIER UCEDA (Life Fellow, IEEE) received the M.Sc. and Ph.D. degrees in electrical engineering from Universidad Politécnica de Madrid (UPM), Spain, in 1976 and 1979, respectively.

He is currently a Full Professor of electronics with the Electrical and Electronic Engineering Department, UPM. His research activity has been developed in the field of power electronics, where he has participated in numerous national and international research projects. As a result of this activity, he has published more than 300 papers in international journals and conferences and holds several national and international patents. His research interests include switched-mode power supplies and dc/dc power converters for telecom and aerospace applications.

Prof. Uceda has received several individual and collective awards, like the IEEE Third Millennium Medal and the Puig Adan Medal. He was awarded an Honorary Doctorate from Universidad Ricardo Palma, Perú, and Colegio de Posgraduados, Mexico.